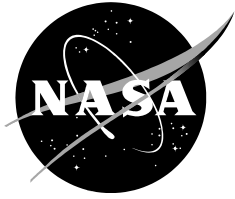# VIPR III VADR SPIDER Structural Design and Analysis

Wesley Li, and Tony Chen
Armstrong Flight Research Center, Edwards, California

September 2016

NASA STI Program ... in Profile

Since its founding, NASA has been dedicated to the advancement of aeronautics and space science. The NASA scientific and technical information (STI) program plays a key part in helping NASA maintain this important role.

The NASA STI program operates under the auspices of the Agency Chief Information Officer. It collects, organizes, provides for archiving, and disseminates NASA's STI. The NASA STI program provides access to the NTRS Registered and its public interface, the NASA Technical Reports Server, thus providing one of the largest collections of aeronautical and space science STI in the world. Results are published in both non-NASA channels and by NASA in the NASA STI Report Series, which includes the following report types:

- TECHNICAL PUBLICATION. Reports of completed research or a major significant phase of research that present the results of NASA Programs and include extensive data or theoretical analysis. Includes compilations of significant scientific and technical data and information deemed to be of continuing reference value. NASA counterpart of peer-reviewed formal professional papers but has less stringent limitations on manuscript length and extent of graphic presentations.

- TECHNICAL MEMORANDUM. Scientific and technical findings that are preliminary or of specialized interest, e.g., quick release reports, working papers, and bibliographies that contain minimal annotation. Does not contain extensive analysis.

- CONTRACTOR REPORT. Scientific and technical findings by NASA-sponsored contractors and grantees.

- CONFERENCE PUBLICATION. Collected papers from scientific and technical conferences, symposia, seminars, or other meetings sponsored or co-sponsored by NASA.

- SPECIAL PUBLICATION. Scientific, technical, or historical information from NASA programs, projects, and missions, often concerned with subjects having substantial public interest.

- TECHNICAL TRANSLATION. English-language translations of foreign scientific and technical material pertinent to NASA's mission.

Specialized services also include organizing and publishing research results, distributing specialized research announcements and feeds, providing information desk and personal search support, and enabling data exchange services.

For more information about the NASA STI program, see the following:

- Access the NASA STI program home page at http://www.sti.nasa.gov

- E-mail your question to help@sti.nasa.gov

- Phone the NASA STI Information Desk at 757-864-9658

- Write to:
  NASA STI Information Desk
  Mail Stop 148
  NASA Langley Research Center
  Hampton, VA 23681-2199
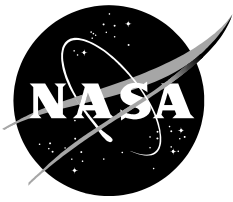
VIPR III VADR SPIDER Structural Design and Analysis

Wesley Li, and Tony Chen
Armstrong Flight Research Center, Edwards, California

September 2016

Abstract

In support of the National Aeronautics and Space Administration (NASA) Vehicle Integrated Propulsion Research (VIPR) Phase III team to evaluate the volcanic ash environment effects on the Pratt & Whitney F117-PW-100 turbofan engine, NASA Armstrong Flight Research Center has successfully performed structural design and analysis on the Volcanic Ash Distribution Rig (VADR) and the Structural Particulate Integration Device for Engine Research (SPIDER) for the ash ingestion test. Static and dynamic load analyses were performed to ensure no structural failure would occur during the test. Modal analysis was conducted, and the results were used to develop engine power setting avoidance zones. These engine power setting avoidance zones were defined to minimize the dwell time when the natural frequencies of the VADR/SPIDER system coincided with the excitation frequencies of the engine which was operating at various revolutions per minute. Vortex-induced vibration due to engine suction air flow during the ingestion test was also evaluated, but was not a concern.

Nomenclature

CL	centerline
D	diameter of shedding body
f	vortex shedding frequency
FEA	finite element analysis
FEM	finite element model
FS	factor of safety
GSE	ground support equipment
MS	margin of safety
MSC	MacNeal-Schwendler Corporation
NASA	National Aeronautics and Space Administration
P&W	Pratt & Whitney
RBE2	rigid bar elements
Re	Reynolds number
RPM	revolutions per minute
SPIDER	Structural Particulate Integration Device for Engine Research
St	Strouhal number
TW	test wing
U	flow velocity
VAE	volcanic ash environment
VADR	Volcanic Ash Distribution Rig
VIPR	Vehicle Integrated Propulsion Research
v	kinematic viscosity

I. Introduction

The National Aeronautics and Space Administration (NASA) Vehicle Integrated Propulsion Research (VIPR) project is a multiagency-industry partnership created in 2010. This project was under the NASA Aeronautics Research Mission Directorate (ARMD) Transformational Aeronautics Concepts Program and the Convergent Aeronautics Solutions Project. The test team involved all four of the NASA aeronautics research centers: Armstrong Flight Research Center (AFRC), (Edwards, California), Ames Research Center (Moffett Field, California), Glenn Research Center (Cleveland, Ohio), and Langley Research Center (North Hampton, Virginia). Major partners from other government agencies and industries included the Federal Aviation Administration (Washington District of Columbia), the Air Force Research Laboratory

(Wright Patterson Air Force Base, Ohio), the 412 Test Wing (TW) of the Air Force Test Center (Edwards, California), the United States Geological Survey (Reston, Virginia), Pratt & Whitney (P&W), (East Hartford, Connecticut), General Electric (Fairfield, Connecticut), and Rolls-Royce (Derby, England, United Kingdom). The primary objective of this project was to help improve the understanding of the impact of volcanic ash ingestion on aircraft engines. In order to meet this project objective, a series of engine ground tests was performed using a Pratt & Whitney F117-PW-100 turbofan engine. The VIPR III was the third phase of the VIPR project, which built upon the results of VIPR Phase I and II to finally start injecting volcanic ash into the engine. The VIPR I testing established engine and sensor performance baselines, while VIPR II was an extension of the VIPR I program. The goal of VIPR III was to accelerate engine life degradation through the ingestion of volcanic ash. This portion of the VIPR III testing was called Volcanic Ash Environment (VAE).

The NASA AFRC VIPR III team was tasked to lead the VAE testing on the P&W F117-PW-100 turbofan engine mounted on pylon 4 of the C-17A airplane (McDonnell Douglas, now The Boeing Company, Chicago, Illinois). Engine 4 is the outboard far right engine from the pilot's perspective as shown in figure 1. The volcanic ash ingestion test was conducted through a series of ground engine runs to simulate prolonged flight through a distal of the volcanic ash cloud. Two of the primary ground support equipment (GSE) required were the Structural Particulate Integration Device for Engine Research (SPIDER), along with the Volcanic Ash Distribution Rig (VADR) and its interfacing hardware to SPIDER. The VADR consisted of a large compressor, a dryer, an ash auger, and ash ducting that directed volcanic ash to the engine inlet. The SPIDER structure was attached from the end of the VADR to the engine casing to ensure that the relative distance between the VADR nozzles and the engine inlet would remain fixed as the engine moved during test operations.

ED15-0188-1128

Figure 1. Overview of the volcanic ash research test setup.

The purpose of this report is to document the structural design and analyses of the SPIDER and the portion of the VADR, near the engine inlet, which would experience considerable loading in the dynamic environment during the test. The structural design and analyses are described in Sections II and III.

II. Overview of VADR-SPIDER Design

The VIPR III ingestion test required the VADR to simulate volcanic ash directed to the engine core. The VADR ducting that delivered the ash near the engine inlet consisted of piping, flexible hose, and the nozzle assembly. The VADR ducting was bolted to a 24-ft diameter circular ground platform which was positioned under the test engine as shown in figure 2. The 5-ton ground platform is heavy enough to prevent any movement in the presence of approximately 3,400 lbf of aerodynamic lift due to engine airflow.
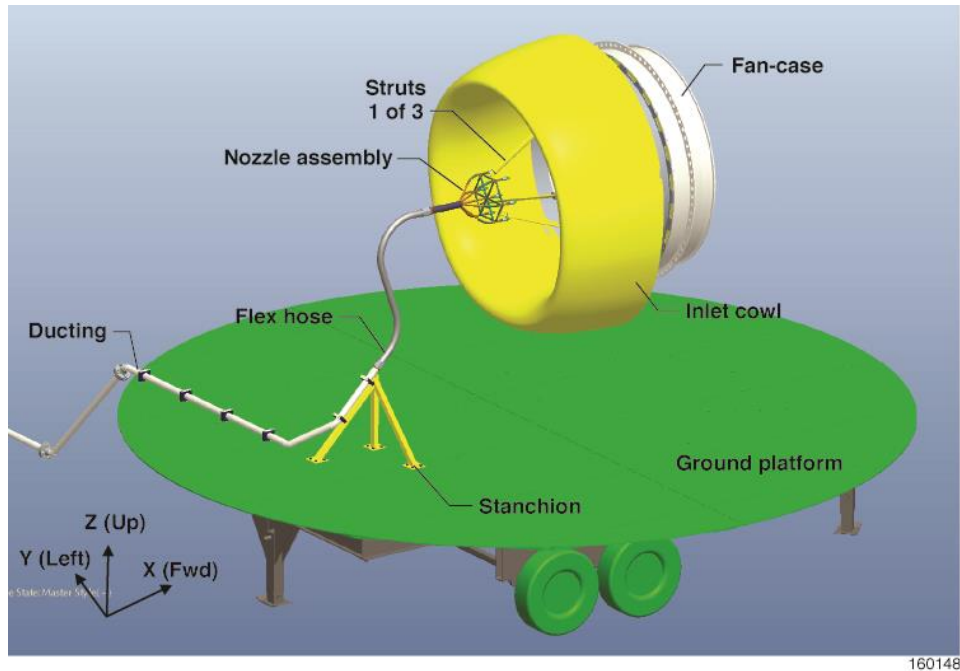

Figure 2. The CAD model of the volcanic ash research test setup.

As shown in figure 3, the VADR nozzle assembly was supported forward of the engine inlet by the SPIDER. The SPIDER consisted of three struts and fittings at both ends that rigidly mounted the VADR nozzle assembly to the fan case. Locking nuts or safety wires were applied to ensure all the connections were secured. This precaution was taken to prevent any hardware from being ingested into the engine. The straight nozzle extension was designed to be 16 in long to enable even distribution of the volcanic ash to the seven nozzles as shown in figure 4. The center nozzle was positioned forward and below the spinner tip near the calculated aerodynamic center for inlet flow as shown in figure 5.

It was expected that the engine would move no more than 6 in due to wind, fuel consumption, and engine thrust. A 75-in long flex hose, which should have sufficient length to accommodate the aircraft movement up to 10 in and yet be able to withstand the high internal pressure, was used to connect the VADR piping to the nozzle assembly. As shown in figure 5, the flex hose was made of T321 stainless steel, annular, corrugated metal hose with a single T304 stainless steel braid, (Hose Master P/N AF4750, HoseMaster LLC, Cleveland, Ohio). The lower end of the flex hose was connected to a rigid pipe and supported by the stanchion mounted on the circular ground platform.
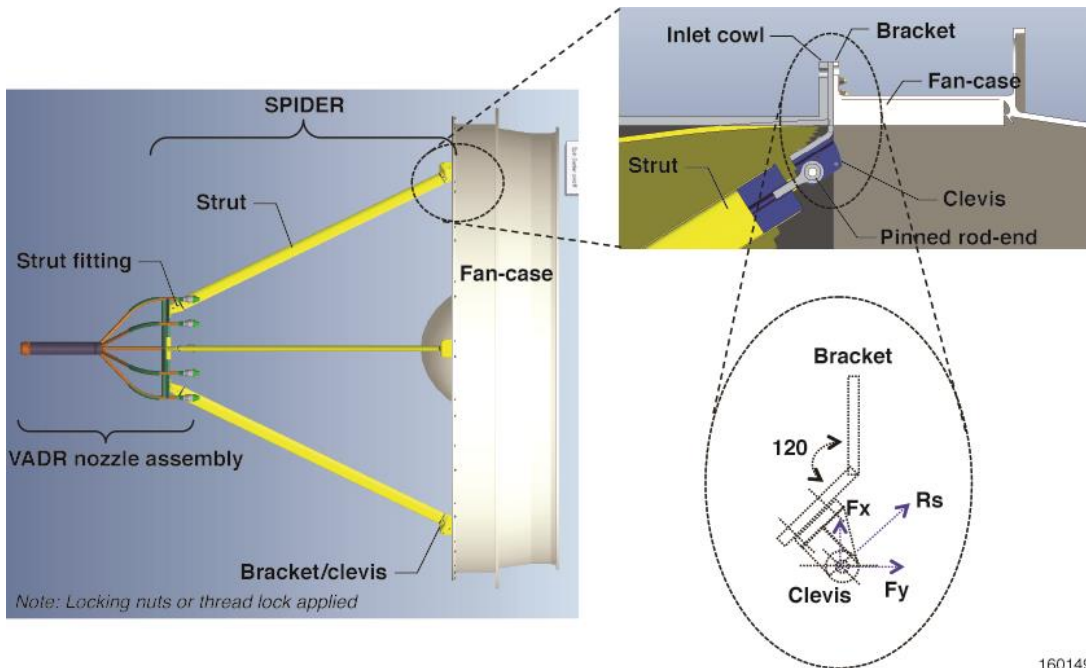
Figure 3. Overview of the VADR/SPIDER design.
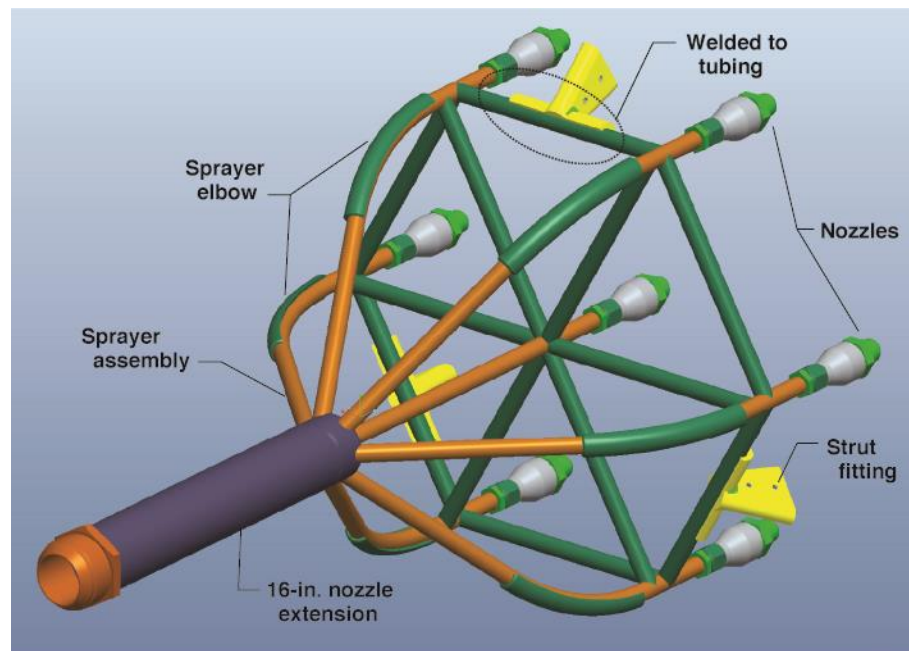
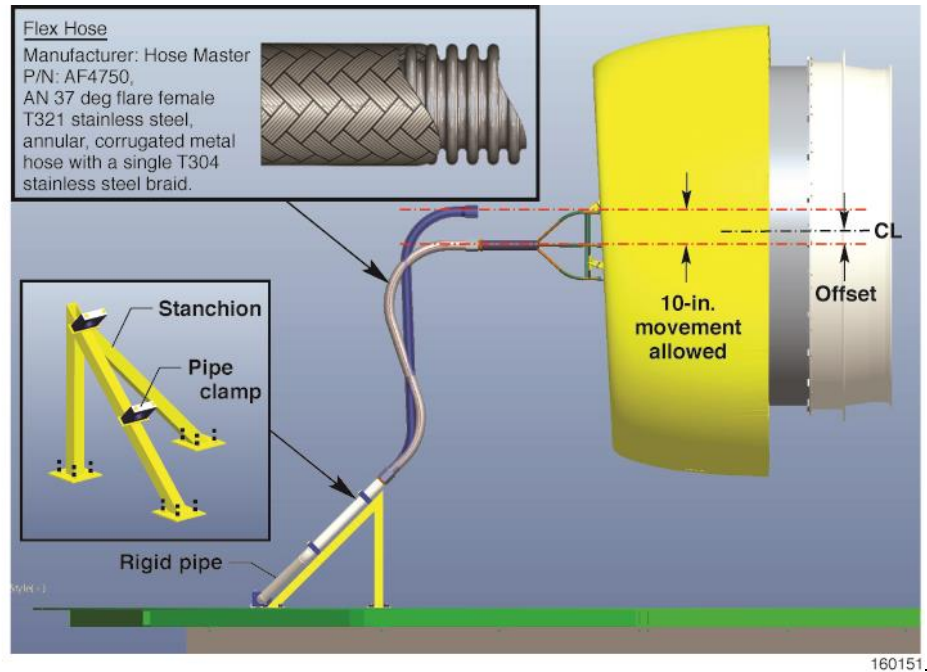Figure 4. Overview of the VADR nozzle assembly.

4

Figure 5. Overview of the VADR flex hose and stanchion design.

The structures between the engine fan case and the test platform were analyzed, and it was predicted that no structural failure would occur during the test. The analyses are described in Section III.

III. Structural Analysis

Several structural analyses of the VADR/SPIDER were performed using both finite element analysis (FEA) and hand calculations. These analyses predicted that the structure had positive structural margins and would not fail or yield under ultimate loads or limit loads, respectively. The VADR/SPIDER structures were subjected to aerodynamic loads, inertia loads, hose tugging loads, and dynamic loads from vibration excitation. The FEA took into account a combination of all these loads.

MSC NASTRAN™ solution 101 (MSC Software Corporation, Newport Beach, California), a static loads analysis solution, was used to determine the loads distribution of the VADR/SPIDER structures. The nodal forces output from the static loads analysis was used for a detailed stress analysis of the rigid connections. Buckling analysis using an empirical approach was used to verify that the struts would not buckle under limit loads.

MSC NASTRAN™ solution 103, a modal analysis solution, was used to determine the modal characteristics (natural frequencies and mode shapes), total weight, center-of-gravity locations, and mass moment of inertia of the VADR/SPIDER. The modal analysis results were essential for developing engine power setting avoidance zones to minimize the duration of the structural excitation at the natural frequencies of the VADR/SPIDER. A vortex-induced vibration assessment was conducted on the strut and the flex hose.

A. Finite Element Model

The VADR/SPIDER design was modeled using PTC Creo® CAD software (PTC, Inc., Needham, Massachusetts). The Finite Element Model (FEM) of the nozzle assembly and struts was generated using MSC PATRAN® (MSC Software Corporation, Newport Beach, California) as shown in figure 6 (ref. 1). The structures were modeled using bar elements (CBAR) with equivalent cross-section properties. The total

number of elements in the FEM was 318. The strut and the engine fan attachments were modeled using rigid bar elements (RBE2) representative of the rigid bolted connections. The strut fitting was also modeled using RBE2 representing the welded connection. The base of the fan case, which assumed to be rigid, was fully constrained and was modelled as fixed ends in all translational and rotational degrees of freedom. The other end of the nozzle assembly connected to the flex hose was modelled as unconstrained. Additionally, a lumped mass was used to represent the weight of the flex hose. In order to ensure that the VADR/SPIDER would be able to withstand the applied loads, it was designed with the use of high-strength metallic materials. The materials and their design allowable used in the analysis are listed in table 1. The total analytical weight of the VADR/SPIDER and the 75-in long flex hose was 41.5 lb. Although the 75-in long flex hose should have sufficient length to accommodate the aircraft movement, as a precaution, two longer hoses (82- and 85-in long) were also considered in the analysis. The weight difference between the 75- and 85-in hoses was 0.86 lb or about a 2.1-percent increase in total analytical weight. The weight of each component is summarized in table 2.

Table 1. Ultimate and yield strength of materials.

Description	Material	Ultimate stress, ksi	Yield stress, ksi
Bracket	4130 AMS 6345	90	70
Clevis	4130 AMS 6345	90	70
Strut	4130 AMS 6361	90	70
Strut lug	4130 AMS 6345	90	70
Nozzle lug	304L ASTM A240	70	25
VADR nozzle assembly	316 ASTM A240	75	30

Table 2. Weight summary of the Volcanic Ash Distribution Rig (VADR).

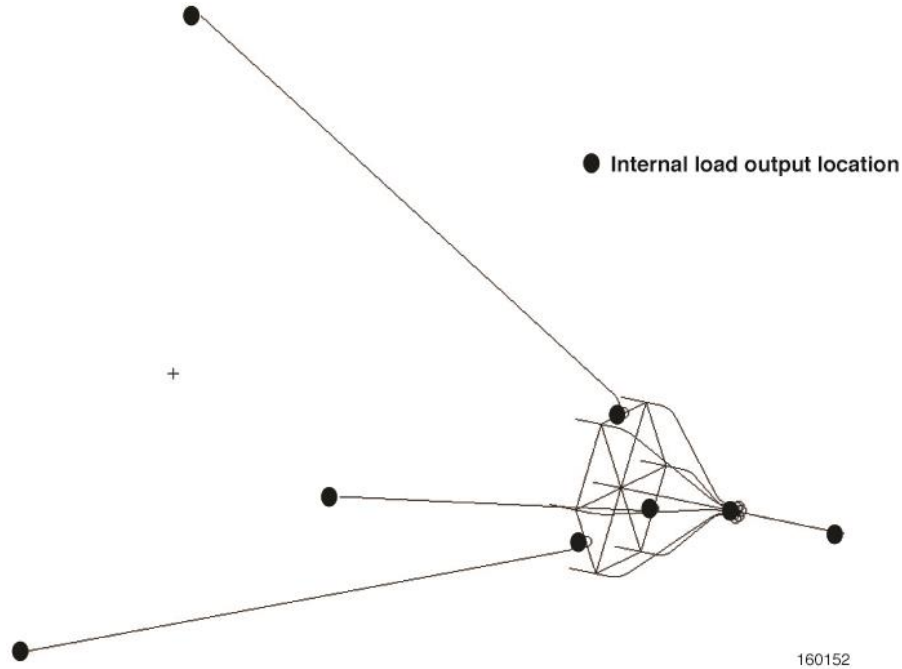| Components	Weight, lb
Struts (3)	13.6
Sprayer assembly	14.9
16-inch nozzle extension	6.0
75-inch flexible hose	7.0
82-inch flexible hose	7.6
85-inch flexible hose	7.9

Figure 6. Finite element model of the VADR/SPIDER.

B. Design Loads

A total of five applied load cases were identified for static loads analysis. The load case number 6 combined all five loads together. The load cases are listed in table 3. These loads included aerodynamic loads, inertia loads, and flex hose nozzle tugging loads. Aerodynamic forces due to the engine airflow were estimated based on a computational fluid dynamics analysis provided by P&W. The inertia load came from the weight of the structure and the flex hose. The tugging loads resulted from the aircraft/engine movement, and the stiffening of the flex hose was caused by the increased internal pressure. The aircraft engine was expected to move a few inches during testing. The pressurized flexible hose would become stiffer and increase in resistance to the movement of the engine and the VADR nozzle assembly. The tugging loads were applied to the end of the 16-in nozzle extension. Given that the VADR nozzle assembly and the SPIDER structures were rigidly attached to the engine fan case and subjected to a dynamic environment, a dynamic load factor of 2.0 was applied to the static loads to account for variance in the loads due to the operating conditions, such as engine vibration, and at the time of engine startups and shutdowns. The maximum engine periodic movement of 0.005 in. peak-to-peak produced by the engine blade imbalance was modeled as input excitation for dynamic load analysis.

Table 3. Design load cases.

Case	Description
1	Aerodynamic load
2	Vertical hose load, 30 lb down
3	Horizontal hose load, 10 lb right
4	Axial hose load, 10 lb aft
5	1.0 g inertia
6	Combined (case 1 to 5)

C. Factor of Safety

The VADR/SPIDER was designed to meet the NASA standard for GSE which required using a design factor of safety (FS) of 5.0. The use of this FS value would eliminate the need of any structural proof load testing and real-time structural loads monitoring during the test. It is practical to design the GSE to such a high FS value because weight usually is not a constraint, and therefore, the GSE should be sized to have almost a zero chance of failure in operation. In fact, with the dynamic load factor of 2, the structures were actually conservatively designed to 10 times of the design limit loads. The definition of ultimate loads and margin of safety are defined in equations (1) and (2). Note that load may refer to force, stress, or strain.

$$\text{Ultimate Load} = \text{Design Limit Load} * \text{Factor of Safety} * \text{Dynamic Load Factor} \qquad (1)$$

$$\text{Margin of Safety} = \frac{\text{Allowable Load (Yield or Ultimate)}}{\text{Design Limit Load} * \text{Factory of Safety (Yield or Ultimate)} * \text{Dynamic Load Factor}} - 1 \qquad (2)$$

IV. Results and Discussion

The structural analyses of the VADR/SPIDER were performed. The margins of safety and the frequencies of the VADR/SPIDER were examined. The results of each structural analysis are discussed in this section.

A. Static Load Analysis

A detailed finite element analysis predicted the stress distribution of the struts and the nozzle assembly. Margins of safety for each of the elements were calculated based on NASTRAN along with hand calculations and were all positive. Although NASTRAN text output files showed detailed loads and stresses, stress contours were used extensively to quickly identify areas of high stress. The maximum combined bar stresses of the VADR/SPIDER are shown in figure 7. Areas of high stress are shown in red. This high stress was mostly due to the 6.0-lb weight of the 16-in nozzle extension, and the 7.0-lb weight of the 75-in long flex hose combined with the tug force at the tip of the nozzle extension fitting. The lowest ultimate MS was 0.26 at the nozzle assembly tubing near the nozzle extension.

The FEM model was also used to determine the distribution of the external loads into the internal structure of each component. The internal loads were extracted in the form of element loads. There were three forces, and three moments at each joint location marked with a black dot as shown in figure 6. These element limit loads were then used to conduct the detailed stress analysis for all joints as well as buckling analysis for the struts. The joint stress analyses included fan-case bracket and clevis, strut fitting bracket clevis and lugs, and nozzle assembly tube-to-tube welds. The MS of the components are summarized in table 4. For the 82- and 85-in long flex hose configurations, the stresses were increased by 2.1 percent for the MS calculation instead of repeating the analysis, since the total analytical weight increase from the 75- to 85-in flex hose configuration was 2.1 percent. This approach was quick and conservative as other loads remained unchanged. The lowest ultimate MS would reduce from 0.26 to 0.23, which remained positive.

The stanchion was made of 2.0-in square steel tubing with 0.25-in wall thickness. Even with a conservative loading of a 200-lb limit load applied in the forward direction and above the upper pipe clamp section, the hand calculations indicated the margin of safety of the stanchion was greater than 60. The stanchion design was sufficient for this test.
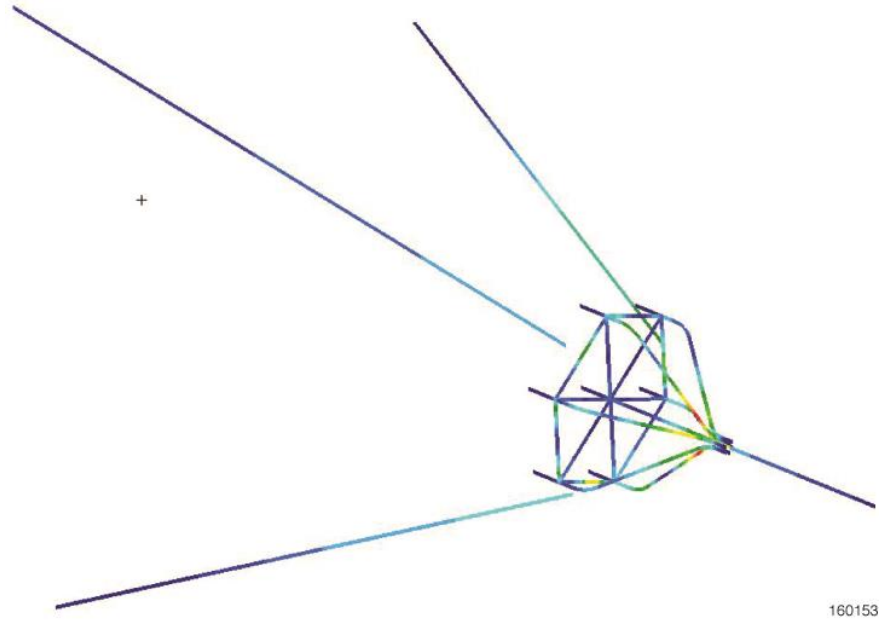
Figure 7. Maximum combined bar stresses of the VADR/SPIDER.

Table 4. Margin of safety of the static analysis of the 75- and 85-inch long flex hose configuration.

Components	Failure mode	Margin of safety	
		75-in flex hose	85-in flex hose
Bracket	Bending	1.5	N/A
Clevis	Hole bearing	23.5	N/A
Clevis	Lug tear-out	36.8	N/A
Fan-case	Bending	5.2	N/A
Strut	Buckling	2.7	N/A
Strut lug	Bearing	16.7	N/A
Nozzle lug	Bearing	14.3	N/A
Support tube, VADR	Bending	1.1	N/A
Nozzle assembly, VADR	Bending	0.26	0.23

B. Modal Analysis

The VADR/SPIDER structure should be free of dynamic frequency couplings to the aircraft lower order modes for the fuselage, wing, and pylon; and the aircraft low order modes will have the most deflection and excitation energy when compared to the higher order modes. The aircraft rigid body modes; wing 1st bending; and the pylon rigid-body modes (pitch, yaw, and roll modes) were considered as the aircraft low order modes. Furthermore, the engine excitation frequencies at various power revolutions per minute (RPM) settings should be considered. If one of the natural frequencies of structure matches or is near the excitation frequencies, the structure would resonate at an amplified amplitude, which may result in structural damage. To minimize the couplings, lowest frequency of the VADR/SPIDER structure should maintain at least a margin of 20-percent frequency separation from the aircraft lower order modes. Modal analysis was performed to determine the modal frequencies and the mode shapes of the VADR/SPIDER

structure. The modal analysis results were then compared with the frequencies of the aircraft lower order modes and the engine RPM frequencies.

During the volcanic ash ingestion test, ash was pumped into the engine through the flex hose at a pressure of 50 psi, which caused the stiffness of the flex hose to increase, and thus changed the natural frequencies of the nozzle assembly/struts. To study this effect, pre-stiffened normal mode analysis with the 75-in flex hose was conducted to simulate both unpressurized and pressurized hose configurations. The resistance of the flex hose was modeled and simulated using applied loads (pre-load) at the nozzle. Two configurations, the unpressurized hose configuration and the pressurized hose configuration, were analyzed, and the modal frequencies were compared. The frequencies for the first ten modes of the hose with a pre-load of 0, 30, and 100 lb, which simulated different internal pressure levels, are summarized in table 5. The results showed that there were only negligible changes in the modal frequencies from no pre-load to 100-lb pre-load. As a result, to simplify the problem, the effect of the pressurized hose was ignored, and the unpressurized hose configuration was used for the dynamic analysis. The first six mode shapes are shown in figure 8.

Table 5. Modal frequency comparison of the unpressurized and pressurized flex hose configuration.

Mode number	Frequency, Hz			Mode shape
	Unpressurized, no applied load	Pressurized, 30 lb down	Pressurized, 100 lb down	
1	21.15	21.14	21.10	Nozzle vertical
2	22.39	22.34	22.23	Nozzle lateral
3	34.66	34.65	34.62	Nozzle torsional
4	37.22	37.23	37.26	Vertical
5	38.94	38.94	38.93	Torsion
6	59.20	59.22	59.26	Strut 1st bending
7	65.59	65.57	65.55	Strut 1st bending
8	69.71	69.65	69.53	Strut 1st bending
9	92.60	92.57	92.49	Strut 2nd bending
10	100.83	100.80	100.72	Strut 2nd bending

10

Mode 1: 21.15 Hz

Mode 2: 22.39 Hz

Mode 3: 34.66 Hz

Mode 4: 37.22 Hz

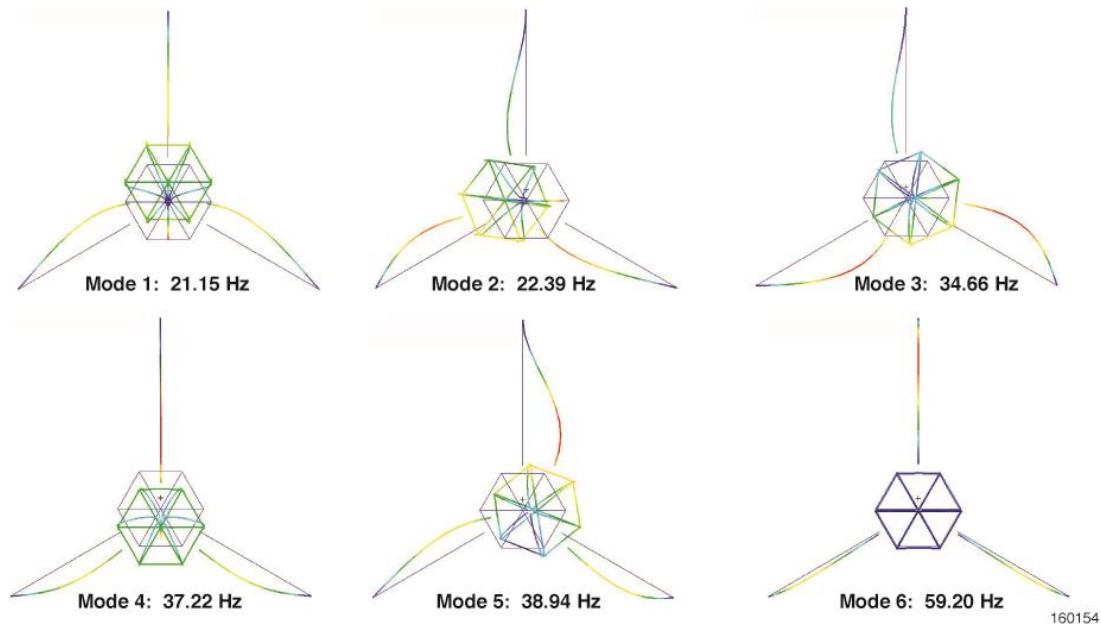Mode 5: 38.94 Hz

Mode 6: 59.20 Hz

160154

Figure 8. The first six natural frequencies and mode shapes of the VADR/SPIDER.

The lower order modes of the C-17 airplane on the ground configuration were unidentified, but estimated to be less than 10 Hz. The first ten modes of the VADR/SPIDER with different flex hose length configurations were calculated and listed in table 6. The lowest natural frequency of the VADR/SPIDER was calculated to be 20.65 Hz (twice that of the 10-Hz aircraft frequency) and well above the natural frequency of the engine idle RPM frequency. As a result, frequency coupling between the aircraft and the VADR/SPIDER, and between idling engine and the VADR/SPIDER was not expected.

Table 6. Modal frequency comparison of the 75-, 82-, and 85-inch long flex hose configuration.

Mode number	Frequency, Hz		
	75-in flex hose	82-in flex hose	85-in flex hose
1	21.15	20.77	20.65
2	22.39	22.01	21.89
3	34.66	34.32	34.21
4	37.22	36.77	36.64
5	38.94	38.82	38.78
6	59.20	59.19	59.19
7	65.59	65.56	65.56
8	69.71	69.69	69.69
9	92.60	92.60	92.60
10	100.83	100.82	100.81

There were no vibration isolator mounts between the engine fan case and struts to reduce the structure vibration transmission. To prevent any undesirable structural vibrations, the results from the modal analysis were used as a guidance for the engine RPM avoidance zones development. The purpose of the zones was to minimize the dwell time when the natural frequencies of the VADR/SPIDER system lined up with the excitation frequencies of the engine, as the engine would be operating at different RPM. The vibration level

was monitored during the test. Sometimes, a few hundred RPM change in operating speed can sufficiently reduce the response to eliminate the unwanted structural vibration problem.

C. Dynamic Load Assessment

Engine blade imbalance could lead to excessive vibration, which for a prolonged period of time would cause structural fatigue and could result in structural failures. Structural dynamics analysis was subsequently conducted to ensure the structural integrity of the VADR/SPIDER structure, which could be excited by the periodic movement of the engine due to engine blade imbalance. Only the first engine mode, which was the engine blade mode and less than 100 Hz, could affect the structure of the system and was considered. The frequency of the second engine mode was above 150 Hz and outside of the first 10 modes of the VADR/SPIDER. With a well-balanced engine blade, the maximum engine periodic movement should be less than 0.005 in. peak-to-peak. The as-measured imbalance for the VIPR test engine was less than 0.0025 in. For this analysis, the engine blade imbalance served as the base excitation for excessive vibration. The base struts with a conservative 0.005 in. peak-to-peak displacement were modeled as input displacement, and 2-percent critical damping was used.

To get to the relatively high engine power setting needed for the ash ingestion test, the engine RPM had to sweep from idle through the power settings that would excite the first few natural frequencies of the VADR/SPIDER. To capture the worst condition, the MS was calculated based on the sum of the bending and axial stress outputs at each of the VADR/SPIDER structure natural frequencies, which assumed the structure was excited at each of the resonance frequencies. Even under those assumptions, the results showed that the structural MS for all the possible resonant conditions were all positive and are summarized in table 7. According to P&W, only the 6th and 7th modes were near the engine operation frequency for this test. Due to the high FS used, the stress levels would be low at resonance and structural fatigue, which was not a concern given the short sweep through durations. This analysis was based on the 75-in flex hose configuration. Although the stresses were increased by 2.1 percent for the 85-in long flex hose configuration, the lowest ultimate MS reduced from 0.06 to 0.04 and remained positive.

Table 7. Margin of safety of the frequency response analysis with 0.005-inch enforced displacement input.

Mode number	Output frequency, Hz	Margin of safety	
		75-in flex hose	85-in flex hose
1	21.15	26.67	N/A
2	22.39	10.49	N/A
3	34.66	0.06	0.04
4	37.22	1.40	N/A
5	38.94	0.10	N/A
6	59.20	9.19	N/A
7	65.59	6.51	N/A
8	69.71	1.67	N/A

D. Vortex-Induced Vibration Assessment

When flowing past a blunt body, such as an airfoil or a circular cylinder, the wake region behind the body usually experiences boundary layer separation and very strong flow oscillations. This regular pattern of vortices in the wake is called a Karman vortex street. The vortex creates an oscillating flow at a discrete frequency that is correlated to the Reynolds number of the flow. The periodic nature of the vortex shedding phenomenon can lead to unwanted structural vibrations and eventually a catastrophic structural failure, especially when the shedding frequency is near or at one of the resonant frequencies of the structure. In general, the first structural mode has the most deflection when excited by the vortex, and therefore, the vortex-induced vibration assessment was conducted by comparing the lower vortex shedding frequency and the first bending mode.

The vortex shedding frequency is a function of the Reynolds number as defined in equation (3):

$$\text{Reynolds number, Re} = \frac{UD}{v} \tag{3}$$

where,
v = kinematic viscosity
D = diameter of shedding body
U = flow velocity

The Reynolds number is based on the diameter of the strut or hose, the flow velocity, and the kinematic viscosity. The dimensionless Strouhal number (St) is used to describe the relationship between the vortex shedding frequency and the flow velocity, as given in equation (4):

$$St = f \times D / U \tag{4}$$

where,
f = vortex shedding frequency
D = diameter of shedding body
U = flow velocity

The kinematic viscosities for air at $80°F$ and $120°F$ were 1.69×10^{-4} and 1.89×10^{-4} ft^2/s, respectively. The diameters of the strut and the flex hose were estimated to be 1.0 and 2.69 in, respectively. Based on the maximum flow velocity estimated for the strut and the flex hose. The Strouhal number equaled approximately 0.2 to 0.3 for the strut and 0.16 to 0.21 for the flex hose (ref. 2). Note that the Strouhal number is not sensitive to the air kinematic viscosity at different temperatures. A parametric study was conducted to cover the uncertainties. The results are listed in table 8. The lowest dimensionless vortex shedding frequencies of the strut and the flex hose were around 840 and 79 Hz, respectively.

The first bending frequency of the Strut (mode 6 in figure 8) was 59.2 Hz, which is much lower than the vortex shedding frequency of 840 Hz. The natural frequency of the flex hose was estimated to be less than 10 Hz, which is less than the 79 Hz shedding frequency. Since the resulting vortex shedding frequencies were not at or near the structural natural frequencies, vortex-induced vibration was not a concern for the struts and the flex hose. In addition, the flex hose, considered to be a high-damping system with its rough surface of a stainless steel braided hose, would act as a vortex generator to delay local flow separation and may prevent the occurrence of the Karman vortex street.

Table 8. Parametric study results of the vortex shedding frequency.

Component	D, inch	U, ft/sec	Reynolds number	Strouhal number	Vortex shedding frequency (f), Hz
Strut	1.0	440	2.17E+05	0.25	1320
	1.0	500	2.47E+05	0.30	1800
	1.0	350	1.73E+05	0.20	840
Hose	2.69	200	2.65E+05	0.21	187
	2.69	110	1.46E+05	0.19	93
	2.69	110	1.46E+05	0.16	79

V. Testing

The VAE test was executed at Edwards AFB, California, from June 2015 through July 2015, and a total of 837 minutes of ash flow testing was accomplished. As expected, engine movement relative to the stationary lower end of the flexible hose was estimated to be less than 4 in, which precluded the VADR piping/stanchion to pull on the engine via the flexible hose. The VADR/SPIDER remained steady under the extremely dynamic environment of combined engine vibration and powerful inlet suction air flow. Post-test examination showed no structural damage.

VI. Conclusion

In support of the NASA VIPR III project to evaluate the volcanic ash environment effects on the F117-PW-100 turbofan engine and other commercial high-bypass turbofan engines, NASA Armstrong Flight Research Center has successfully conducted structural design and analysis on the Volcanic Ash Distribution Rig and the Structural Particulate Integration Device for Engine Research, designated as VADR/SPIDER. The static stress analysis, modal analysis, and dynamic load analysis were performed. The applied loads including aerodynamic loads, inertia loads, and flex hose nozzle reactive loads, plus dynamic loads were considered for the loads analysis. A factor of safety of 5.0 was used for the design and added conservatism in the loads analyses. The structures were analyzed using MSC NASTRAN™ as well as hand calculations. The stress contours were plotted, and maximum stress was found to be below the stress limit. Margins of safety for all the components including joints were calculated, and all were greater than zero, thus the design met the requirement. Vortex-induced vibration due to engine air flow was also evaluated and showed that the vortex shedding frequencies were much higher than the concerned bending frequencies. Thus, there was no concern for vortex-induced vibration due to the engine suction air flow. To minimize the duration of the VADR/SPIDER being excited at resonance with the engine RPM running at different power settings, engine avoidance zones were developed based upon modal analysis results. Overall, the VADR/SPIDER design and analysis tasks have been a success as they performed flawlessly to enable the successful completion of the VAE testing.

References

1. *MSC Nastran 2012.2 Quick Reference Guide*, The MSC Software Corporation, Santa Ana, California, 2012.

2. Blevins, Robert D., *Flow-Induced Vibration*, 2nd ed., Krieger Publishing Company, Malabar, Florida, 2001.